Lasers in Manufacturing Conference 2021

Evaluation of steady state via thermography during laser-directed energy deposition with wire

Anton Odermatt* and Nikolai Kashaev

Institute of Materials Mechanics, Department of Laser Processing and Structural Assessment, Helmholtz Zentrum Hereon, Max-Planck-Straße 1, 21502 Geesthacht, Germany

Abstract

Additive manufacturing of structures in a single continuous deposition process is appealing because defects at the start- and end-points of a track can be avoided. For the evaluation of process stability, a steady state process needs to be reached. A methodology for the determination of the interpass temperature for processes using a positioner for movement of the work piece has been developed. This methodology was applied to a laser- and wire-based directed energy deposition process. The approach of the steady state process can be described by an exponential growth law. From the interpass temperature, a cooling rate can be calculated. The evolution of the interpass temperature can be used for process control and the cooling rate can be related to material properties. A comparison with results from the literature shows that the convergence rate is mainly dependent on the power level of the energy source and the size of the structure.

Keywords: thermography; steady state; process control; interpass temperature; cooling rate

1. Introduction

Wire-fed laser-directed energy deposition (L-DED-wire) has emerged as an additive manufacturing process for large-scale structures in order to realize high build rates of around 0.6 to 0.7 kg/h (Xu et al., 2017; Węglowski et al., 2019; and Elmer et al., 2020), which are mandatory for the manufacture of large-scale steel structures. In order to realise the increased build rates, higher heat inputs are required when compared to laser powder bed fusion (L-PBF). The thermal history during additive manufacturing has a large impact on the quality and properties of the final structure (Carter et al., 2019; Chechik et al., 2021). The exact amount of energy, which is introduced into the part as well as the resultant thermal history, are difficult to quantify, since the relevant physical quantities—such as the absorption, radiation, and convection coefficients, thermal conductivity, specific heat, and latent heat associated with phase transformations—are temperature dependent (Charles Murgau et al., 2019) and difficult to measure (Carter et al., 2019). The most important quantity is the power of the laser, but less obvious factors may also exert great influence. For example, by defocusing the laser beam, the beam irradiance can be adjusted. It is, thereby, possible to influence the aspect ratio and the temperatures of the melt during the L-DED-wire process (Froend et al., 2020). Even if constant process parameters for additive manufacturing are chosen, the temperature distribution and process behaviour can constantly change because of heat conduction and accumulation. Apart from the thermophysical properties of the specific material, the structural design as well as the building strategy, too, exert great

* Corresponding author. Tel.: +49 (0)41 52 87-2507; fax: +49 (0)41 52 87-42536.
E-mail address: anton.odermatt@hereon.de.

influence on the thermal history of a structure. Structures that have a higher surface-to-volume ratio are more affected by radiation and convection. Closed contours, like tubes or rectangular profiles, are subject to cavity radiation phenomena, where the features opposite the current hottest region are heated by the thermal radiation from the melt pool. In order to obtain uniform microstructures and properties within the structure, a steady state during L-DED-wire process is sought, where the temperature field is almost constant and no more adjustment of the process parameters is mandatory. Knowledge of the actual temperature distribution enables not only the control by process parameter adjustments but also allows assessment of the quality of the structure.

The question as to whether this steady state has been reached is relevant for the evaluation of the process stability. Process stability, in this context, means that each deposited layer has the same shape, and undergoes the same cooling rate as the previous one. Reaching a stable process means that it can be continued indefinitely without any change in the process parameters.

Optimizing the process parameters (especially offset per layer and laser power in dependence on the height or the number of tracks) for the production of large structures is often achieved by a time- and material-consuming trial and error approach. Analytical or numerical models are not sufficiently accurate to predict track heights over tens or hundreds of layers, where small errors add up quickly and predictions are often very sensitive to the assumed boundary conditions and parameter settings (Li et al., 2021).

The material properties of specimens taken from regions where a steady state has been reached are likely to be more representative than those from structures where the process has been terminated prematurely. The cooling rate in the first few layers close to the substrate is very different from the cooling rate in the upper regions of the part. This results in differences in microstructure and, hence, variations in mechanical properties along the height of additively manufactured structures. DED processes are envisaged for the production of large-scale parts so that the production of small samples, which have material properties that can be compared to those of larger structures, is relevant for certification purposes.

For example, the standard DIN/TS 17026:2020-10 (DIN, 2020) issues the instruction that the interpass temperature should not vary by more than a certain temperature range for the certification of a parameter set. The interpass temperature has a great influence on the remelting depth, solidification, and cooling rate, and, therefore, the grain size and morphology, which, in turn, determine the mechanical properties (Babkin et al., 2020).

The remelting depth into the previous layer is strongly influenced by the energy introduced and the temperature of the preceding layer during the L-DED-wire process and needs to be controlled (Abbes et al., 2020). If the remelting depth is too low, problems with insufficient bonding with the previous layer may occur. This is, for example, the case if the temperature of the previous layer—which is called the interpass temperature—is lower than assumed and a too-low laser power is chosen for the L-DED-wire process. Other problems may arise from the underestimation of this interpass temperature, where a too-high laser power and, hence, unnecessarily high amounts of energy are introduced into the structure during the L-DED-wire process, leading to unwanted microstructural changes or even process instabilities through overheating of the melt pool (Carter et al., 2019).

Start- and end-points of the L-DED-wire are always possible sites for defects, which can be very detrimental for the properties of the final part. The reasons for the introduction of defects are synchronization errors between the starting and shutting off of laser and wire, the acceleration of the wire, pulling out of the wire from the molten pool at the end of a track, and the difference in the shape of the track when compared to the stationary process. During the movement of the tool to the next start position, the structure also has more time to cool down; here, valuable time is lost. Therefore, it is advantageous to use a single continuous process whenever possible.

With thermocouples, the temperature can only be acquired for fixed positions, as, for example, in the substrate (Lu et al., 2019). In particular, optical temperature measurement techniques proved to be advantageous for additive manufacturing since the successively changing geometry prohibits the use of thermocouples for the determination of temperatures of the additively manufactured structures (Weisz-Patrault, 2020).

In the present study, an approach is described wherein the temperature distribution during the L-DED-wire process is acquired and analysed for the determination of the interpass temperature and the evaluation of whether the steady state has been reached. This information can be used for tailored L-DED-wire process control and for establishing the correlation of the temperature history and properties.

2. Material and Methods

2.1. Materials

The material used in this study was a duplex stainless steel welding wire of 1.2 mm diameter (3Dprint 2209, Böhler welding). The chemical composition is similar to welding wires, which are normally used for the welding of 1.4462 duplex

stainless steel. It has an increased nickel content compared to the base material, to achieve a more balanced austenite-ferrite ratio in the weld metal. According to the producer, the additively manufactured parts can be used without any solution-annealing step. The substrate material was a 42-mm thick, 150 mm by 100 mm block of stainless steel 1.4541.

2.2. Deposition process

The system used in this study consists of a KUKA 6-axis robot and a KUKA DKP 2-axis positioner, a precision wire feeding system by DINSE GmbH, and a coaxial wire feeding optics by Fraunhofer IWS (Fraunhofer-Institut für Werkstoff- und Strahltechnik IWS). During the L-DED-wire process, the alignment of the tool relative to the toolpath was kept constant by the motion of the robot and positioner, which leads to the part being rotated relative to the camera and the tool mostly moving laterally in relation to the camera. The experimental setup and process planning are shown in Figures 1(a) and (b) respectively. The constraint to lateral movement was achieved by the specification of a working plane in the computer-aided manufacturing software. The result is that the XZ plane of the tool coordinate system is always kept parallel to the working plane indicated in Figure 1(b).

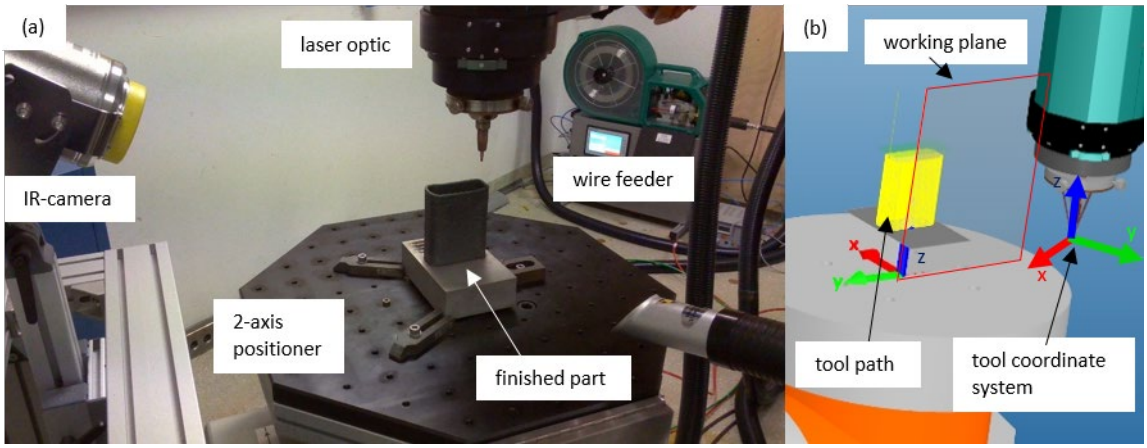

Fig. 1. (a) experimental setup; (b) process planning in the CAM software

The L-DED-wire part has a rectangular footprint (80 mm × 35 mm), with a radius of 10 mm on the corners and a height of approximately 100 mm. The tool path is screw-like, with an offset of 1 mm per layer, which results in a total of 100 layers. The wire fed rate was set to 2 m/min and the welding speed was 0.5 m/min. The power of the laser was held constant at 3.15 kW.

2.3. Temperature measurement

The thermal imaging device is an Optris Pi400 infrared (IR) camera with a 38° lens, which was calibrated for temperatures up to 1500°C. The camera has a resolution of 382 by 288 pixels. The camera was positioned in such a way that the entire part was visible for the whole duration of the process. The resultant distance of 450 mm to the part leads to a resolution of just under 0.9 mm per pixel. The wall of the final part has a width of 4.8 mm, not taking into account the surface roughness. Therefore, a resolution of at least 5 pixels over the thickness of one track is achieved. This resolution would likely be too low to capture the thermal gradients in the melt-pool or the vicinity of the melt-pool, but is sufficient to capture the interpass temperature in accordance with our measurement principle, since the temperature gradients on the side of the structure opposite to the melt-pool are much lower.

For the temperature measurement, a value for the emissivity of 0.65 was used. This value is within the range suggested by the manufacturer (Optris GmbH) for steel surfaces in the expected measurement temperature range. It is likely to be a good estimate for the surface of the substrate. Since the oxidized surface of the additively manufactured part and the melt-pool are likely to have higher emissivity, the emissivity for temperature measurement on the L-DED-wire part was calibrated by comparing the optically measured temperature to a thermocouple measurement. To achieve a temperature similar to the deposition process, the finished part was heated with the defocused laser beam. The best agreement between the measurements by thermocouple and camera was achieved with an emissivity value of 1.0. The high emissivity can be explained by the rough and dark surface of the part and the influence of background radiation from the melt-pool. The emissivity value determined for the additively produced surfaces was used to correct the measured temperature values via

the Stefan-Boltzmann law (Eq. (1)). The corrected temperature T_{corr} in Eq. 1, measured with the assumption of an arbitrary emissivity ε_m, can be calculated from the measured temperature T_m if the real emissivity ε_{corr} is known.

$$T_{corr} = \sqrt[4]{\frac{\varepsilon_m}{\varepsilon_{corr}}} T_m \tag{1}$$

The data acquisition rate was 1 fps. According to the manufacturer, the distance of approximately 450 mm from the camera lens to the part results in a resolution of just under 0.9 mm per pixel. The wall of the final part had a maximum width of 4.8 mm. This results in a resolution of 5 pixels over the thickness of one track.

3. Results

Owing to the coordinated motion of the robot and positioner through the constraint to the working plane (Figure 1(b)), the process zone is always located in the upper part of the thermal images (Figure 2(a)). When a temperature profile along the *y*-axis of the thermal images is extracted, the side opposite to the current process zone is always included and not obscured by the wire-feeding nozzle (green arrow in Figure 2(a)). The position of the evaluation line was identified as the median value of the *x*-position of the pixels with the highest temperature values. The evaluation along a vertical line is a result of the orientation of the working plane of the tool. The entire height of the thermal images was evaluated to ensure that the additively manufactured part is always within the evaluated region. Since the temperature values in the melt-pool exceed the temperatures that can be resolved by the camera, no data was acquired in this region; hence, the evaluation line is always slightly behind the actual melt-pool.

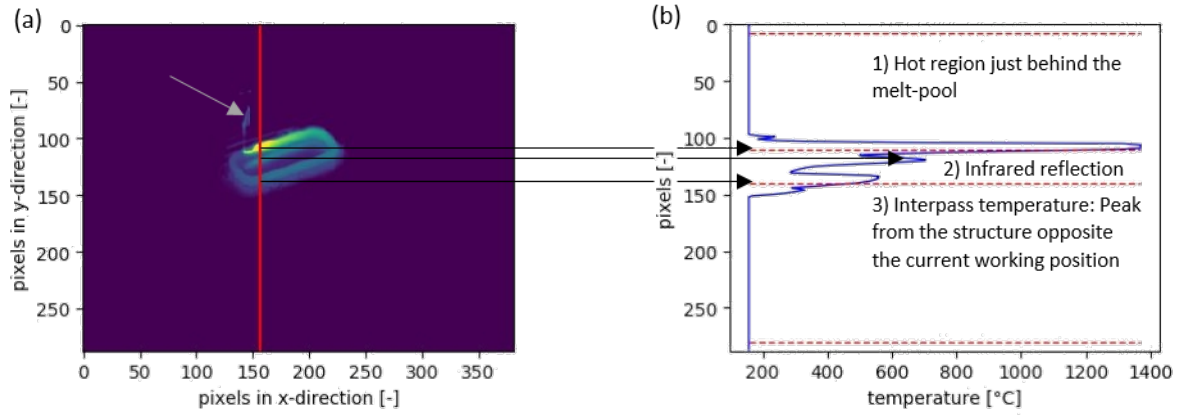

Fig. 2. (a) Thermal image from the L-DED-wire process. A red line highlights the evaluation line. Some reflections of the thermal radiation on the substrate and the wire nozzle (green arrow) are visible. (b) Thermal profile extracted from the process at $t = 180$ s showing the three characteristic peaks from the process zone, reflection at the base, and the structure on the opposite side of the process zone.

A temperature profile was extracted along the evaluation line (Figure 2(b)). This temperature profile exhibits multiple characteristic peaks. The highest peak stems for the evaluation position. At the beginning of the L-DED-wire process, there are three peaks: the first one from the evaluation position, the second one from thermal radiation and reflection near the base of the part under the process zone, and the third one from the opposite side. Theses peaks can be differentiated by their width. While the peaks from the top of the opposite sides of the part are fairly broad, the peak from the reflection at the base is much sharper. Hence, the peak belonging to the current interpass temperature (Figure 2(b)) can be identified by performing a continuous wavelet transform with the wall thickness in pixels and identifying the ridge lines in the wavelet transform matrix. This procedure was developed by Du et al. for the identification of peaks in mass spectrometry (Du et al., 2006).

Owing to the rectangular shape of the structure built in this study, the evaluated position is not always the same distance along the tool path from the current working position. When the temperature is evaluated more on the left side in the thermal image (Figure 2(a)), lower temperatures are measured than on the right side. Hence, the measured interpass temperature oscillates (Figure 3(a)). In order to flatten these oscillations, a continuous function (Eq. 2) is fitted to the time-temperature profile ($T_{i,m}$, Figure 3(a)).

During the L-DED-wire process, thermal energy is continuously put into the part as well as the substrate, and is conducted throughout the structure. In addition, the geometry changes from a block-like (shape of the substrate) at the beginning to a pipe-like (shape of the additively manufactured structure; see Figure 1) in the steady state. The heat-up and change in geometry lead to a transition in cooling behaviour and temperature from an initial state to a final, steady state. In the beginning, the cooling rates are high and the temperature of the substrate is low, because the initial substrate temperature is the room temperature.

Processes that evolve from an initial to a steady state can often be described by a simple exponential growth law (Eq. 2). The interpass temperature development of continuous DED processes that converge to a steady state can be described by such an exponential equation, where T_∞ is the upper limit and steady state value and T_s starting value of the process. The parameter η describes the rate at which the steady state is approached and t_0 is the start time of the process.

$$T(t) = T_\infty - (T_\infty - T_s)e^{-\eta(t-t_0)} \tag{2}$$

The parameter optimization was performed based on the least squares method, by fitting Eq. 2 to the measured data ($T_{i,m}$, Figure 3(a)).

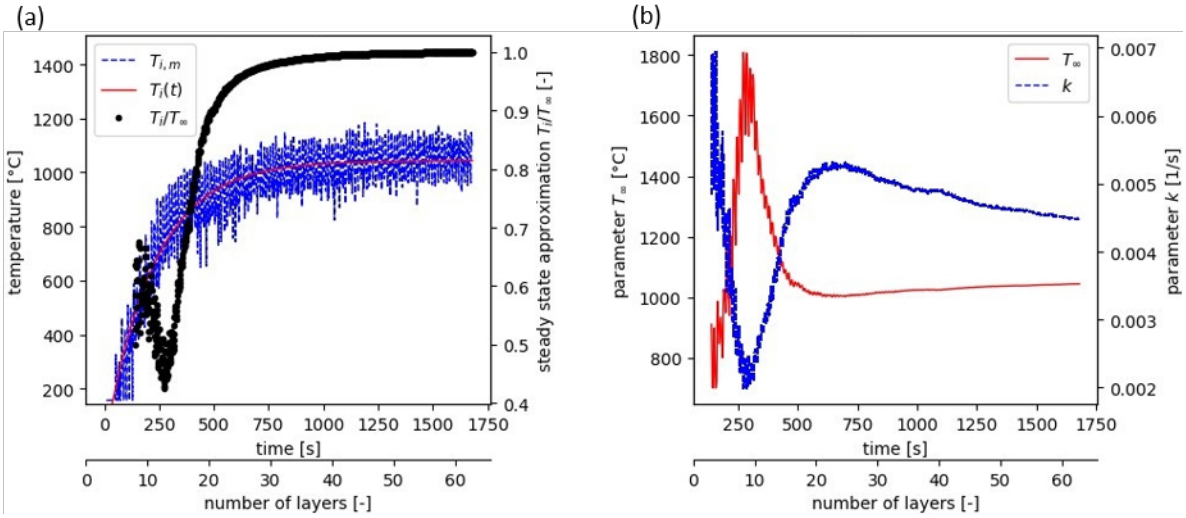

Fig. 3. (a) Measured interpass temperature (blue line), fit function to the measured temperature (orange line), and the steady state approximation (current temperature divided by the upper limit determined by the current value of the fitting parameters). The change in the steady state approximation at the beginning of the build corresponds to a change in the fitted steady state value T_∞. (b) Evolution of the current value of the fitting parameters with time. Only the first 60 layers are shown to achieve better visibility of the transitive regime.

At the beginning of the L-DED-wire process, the optimized values for the free parameters change considerably. After about 700 seconds, or 25 layers, the interpass temperature reaches 95% of the steady state temperature and the predicted threshold temperature nearly converges.

From the maximum temperature (solidus temperature, T_{max}), the current interpass temperature ($T_i(t)$), welding speed (v_s), and length of the tool path for half a revolution (l_t), a cooling rate can be derived through Eq. 3 (Figure 4(a)):

$$k(t) = \frac{(T_{max} - T_i(t))v_s}{l_t} \tag{3}$$

During the process investigated in this paper, the cooling rate reduces from ca 73 K/s to 25 K/s, which is an almost threefold reduction. The cooling rate can be compared to the microstructure formed at certain position of the sample.

Representative cross-sections from the bottom and the top of the deposited structure are presented in Figures 4(b) and (c), respectively. The visibility of the microstructure was enhanced by etching of the polished cross-sections with Beraha II reagent for 5 seconds. As a result the ferrite can be discerned by its dark colour, while austenite remained mostly light. The austenite in Figure 4 (c) appears much darker, since both cross-sections were etched at the same time, but the pictures were taken from bottom to top. Therefore, remnants of the etchant continued to act upon the sample.

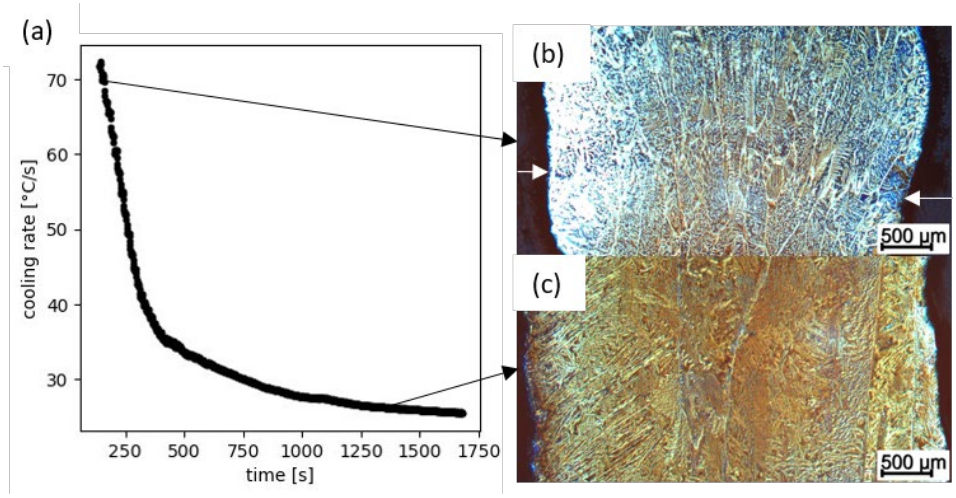

Fig.4. (a) Cooling rate between solidus temperature and current interpass temperature, (b) fine-grained prior ferrite grains from the bottom of the structure and slightly darker layer bands (white arrows), (c) coarse-grained epitaxially grown prior ferrite grains from the top of the structure.

The microstructure in the bottom of the structure (Figure 4(b)) consists of prior ferrite grains, which are discernible by the austenitic grain boundaries separating them, and a network of austenitic needles in the prior ferrite grains. There are between 15 and 20 prior ferrite grains across the cross-section from the bottom. In the cross-section from the top, that number has reduced to five at most (Figure 4(c))). While the height of the prior ferrite grains in the bottom is less than one layer height, the height at the top can be much larger than several layers. In the bottom of the structure darker bands, separating individual layers are barely discernible. These are no longer discernible near the top of the structure. Microstructural defects are not visible in Figures 4 (b) and (c)

4. Discussion

In this study, a new evaluation scheme for the interpass temperatures in continuous L-DED-wire processes is presented. The predictions of the steady state value for the process at hand converged after about 600 s, while the interpass temperature reached 95% of the steady state value (1020°C) after 700 s. During the first 500 seconds of the process, the results of the least-squares fit change considerably. A good prediction of the steady state, based on the transitive regime of the process is, therefore, unlikely.

The increase in the interpass temperature and change in geometry leads to an almost threefold reduction in the cooling rate from 73°K/s to 25°K/s. The remelting depth is likely increased with increasing height because of the increased temperature of the substrate material, which explains the disappearance of the darker bands between layers. The epitaxial grain growth across layers and the resulting increase in size and aspect ratio of the grains has been widely reported on (DebRoy et al., 2018).

The transitive behaviour of the part temperature has been indirectly reported on by other researchers. Kledwig et al. (Kledwig et al., 2019) reported a transition from an initial temperature signal from the melt pool to a steady state signal during the laser powder-fed directed energy deposition of a stainless steel (X2CrNiMo17-12-2). They found that a steady state signal from thermal images of the melt pool was reached after about 400 s of the process. The tool path for one revolution was slightly longer (314 mm) than in the present study (213 mm), but the final height of the part was smaller. In combination with the slightly higher power and material addition rate used, this leads to a 177% higher power per unit length of revolution ((5.7 W/mm vs. 10.1 W/mm) in our study. After 700 s of process in the present study is close to (>95%) approaching the steady state, which is 175% of the time from (Kledwig et al., 2019). Since the structures in the work of Kledwig et al. (Kledwig et al.) are slightly larger compared to the structures in this study, there is a larger area where energy can be transmitted to the surroundings via radiation and convection. At the same time, a lower power of the energy source leads to a lower temperature, at which an equilibrium between introduced, radiated, and convected energy is reached. In

addition to the time to a steady state process, the part level thermography is able to measure the actual interpass temperature and calculate a cooling rate, which can be directly linked to material properties through the resultant microstructure and the remelting depth.

The measurement of optical radiation from the melt-pool is more challenging than on a part level because of the higher temperatures, strong temperature dependency of emissivity, and high resolution required to capture the actual temperature distribution. In addition, if the laser power is controlled via temperature measurements of the melt pool, the optical emission is likely to stay more constant throughout the process. Therefore, the ascertainment of reaching a steady state is hindered by the adjustment of the power. A part-level evaluation is then more promising.

Chechik et al. computed cooling rates of the melt-pool during a DED process with laser and powder from infrared images of the melt pool (Chechik et al., 2021). They found that the cooling rate decreased to a plateau over the first 20 layers, with the effect being more pronounced when a high line energy is employed. This gives merit to the idea of applying an exponential growth law like Eq. 2 to DED processes. In addition, the hardness of their structures correlates with their computed cooling rate.

The computation of cooling rates from the temperature field of the melt-pool should not be the only parameter with which microstructure is predicted. The interpass temperature could have stronger correlation with the remelting depth and the probability of lack of fusion defects. In addition, when the laser power is controlled to keep the melt-pool temperature constant, attempts to judge whether a steady state has been reached cannot be made on the basis of temperature measurements of the melt-pool.

5. Conclusion

The temperature measurements presented in this study have implications for the evaluation of process stability and the estimation of the steady state interpass temperature values of continuous L-DED-wire processes. The methodology presented in this paper is robust as regards the measurement and evaluation procedure, easy to implement, and nearly independent of the part geometry. The only requirement is that the melt pool and the opposite side of the structure are not shrouded from the view of the camera. Owing to the fitting procedure, the determined temperature is fairly stable, even when the evaluated position on the circumference changes because of the part not being perfectly circular, lateral movement of the tool, or off-centric position of the part on the positioner. It is suitable for the evaluation interpass temperatures in continuous DED processes, where the evaluation of thermography data is complicated by the high temperatures of the melt pool and its surroundings. The methodology can be easily adapted for more complex tool paths, as multiple peaks can potentially be evaluated and the one that is most suitable for a description of the process can be chosen.

The rate of convergence to a steady state and the actual temperature values mainly depend on three parameters: the laser power, the size of the structure, and the surface-to-volume ratio. The laser power controls the amount of energy introduced into the structure and the size along with the surface-to-volume ratio control the power that can be radiated and convected away from the structure.

In our future work, we aim to apply the methodology to more parts and different processing conditions, so as to evaluate its effectiveness in linking microstructure with the temperature evolution during the L-DED-wire process.

Acknowledgements

The authors would like to thank Dr. Josephin Enz and René Dinse from the Helmholtz-Zentrum Hereon for support in L-DED-wire experiments and invaluable discussions.

References

Xu, X., Mi, G., Luo, Y., Jiang, P., Shao, X., and Wang, C., 2017. Morphologies, microstructures, and mechanical properties of samples produced using laser metal deposition with 316 L stainless steel wire. Optics and Lasers in Engineering 94, p. 1.

Węglowski, M. S., Błacha, S., Jachym, R., Dutkiewicz, J., Rogal, Ł., Antoszewski, B., et al., 2019. Electron and Laser Beam Additive Manufacturing with Wire—Comparison of Processes. Key Engineering Materials 799, p. 294.

Elmer, J. W., Gibbs, G., Carpenter, J. S., Coughlin, D. R., Hochnadel, P. A. T., Vaja, J. A. Y., et al., 2020. Wire-Based Additive Manufacturing of Stainless Steel Components. Welding Journal 99, p. 8.

Carter, W., Masuo, C., Nycz, A., Noakes, M., and Vaughan, D., 2019. Thermal process monitoring for wire-arc additive manufacturing using IR cameras. Solid Freeform Fabrication 2019: Proceedings of the 30th Annual International Solid Freeform Fabrication Symposium—An Additive Manufacturing Conference, SFF 2019.

Chechik, L., Boone, N. A., Stanger, L. R., Honniball, P., Freeman, F., Baxter, G., et al., 2021. Variation of texture anisotropy and hardness with build parameters and wall height in directed-energy-deposited 316L steel. Additive Manufacturing 38, p. 101806.

Charles Murgau, C., Lundbäck, A., Åkerfeldt, P., and Pederson, R., 2019. Temperature and Microstructure Evolution in Gas Tungsten Arc Welding Wire Feed Additive Manufacturing of Ti-6Al-4V. Materials 12, p. 3534.

Froend, M., Ventzke, V., Dorn, F., Kashaev, N., Klusemann, B., and Enz, J., 2020. Microstructure by design: An approach of grain refinement and isotropy improvement in multi-layer wire-based laser metal deposition. Materials Science and Engineering A 772, p. 138635.

Li, J., Li, H. N., Liao, Z., and Axinte, D., 2021. Analytical modelling of full single-track profile in wire-fed laser cladding. Journal of Materials Processing Technology 290, p. 116978.

DIN/TS 17026 Unbefeuerte Druckbehälter - Zusätzliche Anforderungen an additiv gefertigte Druckgeräte und deren Bauteile. Beuth Verlag GmbH, Berlin. 2020–10.

Babkin, K., Zemlyakov, E., Ivanov, S., Vildanov, A., Topalov, I., and Turichin, G., 2020. Distortion prediction and compensation in direct laser deposition of large axisymmetric Ti-6Al-4V part. Procedia CIRP 94, p. 357.

Abbes, B., Anedaf, T., Abbes, F., and Li, Y., 2020. Direct energy deposition metamodeling using a meshless method. Engineering Computations (Swansea, Wales) ahead-of-print, p. 129.

Lu, X., Lin, X., Chiumenti, M., Cervera, M., Hu, Y., Ji, X., et al., 2019. Residual stress and distortion of rectangular and S-shaped Ti-6Al-4V parts by Directed Energy Deposition: Modelling and experimental calibration. Additive Manufacturing 26, p. 166.

Weisz-Patrault, D., 2020. Fast simulation of temperature and phase transitions in directed energy deposition additive manufacturing. Additive Manufacturing 31, p. 100990.

Fraunhofer-Institut für Werkstoff- und Strahltechnik IWS. *Laser-Bearbeitungsoptik COAXwire: Beschichten, Reparieren und Generieren mit Massiv- und Fülldraht*. Accessed November 26, 2020, https://www.iws.fraunhofer.de/content/dam/iws/de/documents/publikationen/infoblaetter/700-2_COAXwire_de.pdf

Optris GmbH. *Basic principles of non-contact temperature measurement*. Accessed November 26, 2020, https://www.optris.global/infrared-basics

Du, P., Kibbe, W. A., and Lin, S. M., 2006. Improved peak detection in mass spectrum by incorporating continuous wavelet transform-based pattern matching. Bioinformatics (Oxford, England) 22, p. 2059.

International Molybdenum Association, 2014. *Practical Guidelines for the Fabrication of Duplex Stainless Steels*. London, UK.

Debroy, T., Wei, H.L., Zuback, J.S.. Mukherjee, T., Elmer, J.W.m Milweski, J.O., Beese, A.M., Wilson-Heid, A., De, A., Zhang, W., 2018, Additive manufacturing of metallic components – Process, structure and properties. Progress in Materials Science 92, p. 112

Kledwig, C., Perfahl, H., Reisacher, M., Brückner, F., Bliedtner, J., and Leyens, C., 2019. Analysis of Melt Pool Characteristics and Process Parameters Using a Coaxial Monitoring System during Directed Energy Deposition in Additive Manufacturing. Materials (Basel, Switzerland), p. 12.